Early chronic kidney disease-mineral bone disorder stimulates vascular calcification

Yifu Fang, M.D.[1], **Charles Ginsberg**[1], **Toshifumi Sugatani, Ph.D.**[1], **Marie-Claude Monier-Faugere, Ph.D.**[2], **Hartmut Malluche, M.D.**[2], and **Keith A Hruska, M.D.**[1]

[1]Departments of Pediatrics, Pediatric Nephrology Division, Washington University Saint Louis, Missouri

[2]Medicine, Division of Nephrology, University of Kentucky Lexington, Kentucky

Abstract

The chronic kidney disease-mineral and bone disorder (CKD-MBD) syndrome is an extremely important complication of kidney diseases. Here we tested whether CKD-MBD causes vascular calcification in early kidney failure by developing a mouse model of early CKD in a background of atherosclerosis stimulated arterial calcification. CKD equivalent in glomerular filtration reduction to human CKD stage 2 stimulated early vascular calcification and inhibited the tissue expression of α-klotho (klotho) in the aorta. In addition, osteoblast transition in the aorta was stimulated by early CKD as shown by the expression of the critical transcription factor, RUNX2. The ligand associated with the klotho-fibroblast growth factor receptor complex, FGF23, was found to be expressed in the vascular media of sham operated mice. Its expression was decreased in early CKD. Increased circulating levels of the osteocyte secreted proteins, FGF23, and sclerostin may have been related to increased circulating klotho levels. Finally, we observed low turnover bone disease with a reduction in bone formation rates more than bone resorption. Thus, the CKD-MBD, characterized by cardiovascular risk factors, vascular calcification, increased circulating klotho, FGF23 and sclerostin levels, and low turnover renal osteodystrophy, was established in early CKD. Early CKD caused a reduction of vascular klotho, stimulated vascular osteoblastic transition, increased osteocytic secreted proteins, and inhibited skeletal modeling producing the CKD-MBD.

INTRODUCTION

The chronic kidney disease – mineral and bone disorder (CKD-MBD) syndrome is an extremely important complication of kidney diseases. The CKD-MBD was named in 2006[1] following the realization that the mineral and skeletal disorders accompanying kidney failure are important contributors to the CKD associated cardiovascular disease and high mortality

Corresponding Author: Keith A. Hruska, MD, Division of Pediatric Nephrology, Department of Pediatrics, Washington University, 660 S. Euclid Ave., Campus Box 8208, St. Louis, MO 63110, Telephone: 314 286 2772, Fax: 314 286 2894, hruska_k@kids.wustl.edu.

rates.[2-5] Recent studies have suggested that the CKD-MBD defined as biochemical abnormalities in mineral metabolism, abnormalities in skeletal remodeling, and extraskeletal calcification are present when the glomerular filtration is reduced by more than 40%.[6] Within the concept of the CKD-MBD, recent progress related to cardiovascular disease risk factors stimulated by kidney disease has uncovered three: vascular calcification, phosphorus (Pi) and fibroblast growth factor 23 (FGF23).[7-11] Vascular calcification particularly poses increased risk of cardiovascular and all-cause mortality,[7, 12] and of the clinical conditions associated with vascular calcification, the most extensive calcifications occur in CKD.[13] In CKD, vascular calcification is stimulated by hyperphosphatemia and positive calcium balance.[14-18]

Emerging data indicate that the (CKD-MBD) syndrome may begin early in the course of kidney disease and precede the development of clinically detectable abnormalities in plasma phosphorus, calcium, parathyroid hormone and calcitriol, which are the hallmarks of the established CKD-MBD. Biomarkers of skeletal osteocyte function have been found to be abnormal early in kidney disease both clinically and in translational models,[6, 19-23] indicating that kidney injury had affected the skeleton, in other words the CKD-MBD had begun. Pereira et al,[19] found by skeletal immunocytochemistry and plasma levels that osteocyte production of fibroblast growth factor 23 (FGF23) and dentin matrix protein-1 (DMP-1) were increased in stage 2 CKD. These results were confirmed by Sabbagh et al and Oliveira et al,[21, 22] who also found that osteocyte sclerostin was increased in early CKD, and that osteocyte nuclear beta-catenin was decreased indicating decreased osteocyte Wnt activity in early CKD. Since Wnt activity is the major skeletal anabolic principle of the postnatal skeleton[24, 25] these results indicate that kidney disease signals a decrease in bone formation. Fang et al,[20] showed in a translational model of early CKD, elevated FGF23 levels in the presence of normal plasma Ca, Pi, PTH and calcitriol, and a decrease in bone formation rates. These results confirmed earlier reports prior to FGF23 studies from our laboratory that when Ca, Pi, calcitriol, and PTH were maintained normal in CKD, decreased bone formation rates and the adynamic bone disorder were observed.[26] However, it is unknown whether vascular calcification and renal osteodystrophy produced by kidney disease[27, 28] are present in the early stages of the CKD-MBD.

The present studies were conducted to test the hypothesis that the CKD-MBD begins early in kidney disease including the onset of heightened cardiovascular risk related to vascular calcification. We developed an animal model of early CKD using the atherosclerosis bearing low density lipoprotein deficient mouse (*ldlr*−/−) fed high fat Western type diets (40% of calories from fat). The phenotype of these mice is further characterized by insulin resistance progressing to type 2 diabetes over time. The mice respond as humans to atherosclerosis with neointimal plaque calcification which is stimulated by advanced CKD.[29] Using inulin clearances to determine GFR, we staged CKD in mice and developed a model of CKD equivalent in GFR to stage 2 human CKD using unilateral renal injury and contralateral nephrectomy. This model mimics acute kidney injury (aki) and incomplete recovery in humans with atherosclerosis and insulin resistance/diabetes. The peak glomerular filtration rate (representing a 25-40% decrease from normal GFR) established after recovery from acute kidney injury slowly diminished over weeks related to interstitial inflammation and

fibrosis allowing development of the CKD-MBD. Using this model we characterized the early CKD-MBD discovering stimulated vascular calcification in early CKD prior to hyperphosphatemia. The discovery of vascular calcification, early in CKD produced a requisite search for mechanisms, and we discovered mesenchymal transition in vascular cells and newly recognized abnormalities in the arterial tree that cause vascular calcification, reduction of vascular klotho,[30][32] expression of FGF23, and increased circulating klotho. The elevations in circulating klotho (c-klotho) explain the early stimulation of skeletal osteocytes and FGF23 secretion independent of changes in the serum phosphorus.

RESULTS

Studies in early CKD

The overall experimental design is shown in Figure 1. The serum/plasma chemistries (BUN, Ca, Pi and PTH) determined in the experimental groups are shown in Table 1. The BUN of wild-type and sham operated mice ranged from 20 to 23mg/dl (Table 1). In mice with mild renal ablation referred to in this paper as CKD-2, the mean BUN of the group was not elevated at 22 weeks and only increased to 24-30 mg/dl at 28 weeks (CKD-2-28). Inulin clearances confirmed a 33% reduction in GFR in the 22wk *ldlr*–/–CKD-2 group (Figure 2). A 40% reduction from normal GFR is the low end of the GFR range in human stage 2 CKD. The CKD-2 animals were normocalcemic and normophosphatemic at 22 weeks (Table 1). In the 28 wk CKD-2-28 animals, compatible with the slight progression of the kidney insufficiency, hyperphosphatemia had developed (12.7±3.9 mg/dl). These findings are compatible with our previous findings of hyperphosphatemia in mice with more severe ablation and GFR in the human stage 3 CKD range.[14, 33] PTH levels were elevated to 120±48 in the CKD-2 animals at 22 weeks, but were only 90.8±20 pg/ml at 28 weeks (not significantly different from the normal levels of the sham operated animals). The elevation of PTH at 22 weeks in the CKD-2/3 groups following mild renal injury suggests that the elevation may have been related to changes associated with the acute kidney injury phase of the model. As shown in Figure 3A, longitudinal analysis of PTH levels demonstrated 3 fold elevations of PTH during the acute kidney injury phase (15 weeks, one week following surgery) that progressively diminished to levels insignificantly elevated from normal at 28 weeks.

Plasma FGF23 levels measured by the Kainos intact hormone assay were elevated by CKD-2 (Figure 3B). FGF23 levels were progressively increased from 15 to 22 weeks in the face of normophosphatemia, and continued to rise with the development of hyperphosphatemia in CKD-2-28 instead of diminishing similar to PTH levels, and compatible with FGF23 being the basis for the decrease in PTH levels.[34] Use of a domestic FGF23 assay detecting the c-terminus of FGF23 (Immunotopics, Stillwater, MN) demonstrated elevated levels similar to the intact hormone assay at 28 weeks in the CKD-2-28 group (Figure 3C and D). These results suggest the role of FGF23 in maintaining phosphate homeostasis in early CKD.

Aortic and large artery calcification is a critical component of the CKD-MBD producing vascular stiffness and increased cardiovascular disease in CKD.[35] Vascular calcification in the CKD-2 mice was studied by histology and determination of the aortic calcium content in

mg/g dry weight. The CKD-2-28 mice had aortic medial narrowing and advential hyperplasia, but there was no clear evidence of calcium deposition in the media by alizarin red (Figure 4) or the less sensitive von Kossa (not shown) staining. Aortic Ca content was significantly increased in the CKD-2-28 mice compared to the sham operated control mice (Figure 4B), and we observed detectable increases in the neointimal atherosclerotic plaque calcium deposits as shown below for the CKD-3-28 mice similar to that we have previously reported in stage 4 CKD.[29]

Osteoblastic transition of neointimal cells in atherosclerotic lesions has been shown to be critical in the pathogenesis of vascular calcification stimulated by CKD-3-28 in the *ldlr*−/− high fat fed mouse model,[36] and others using different models have shown that osteoblastic transition is involved in medial calcification.[13, 37, 38] Therefore, we examined whether cells in the aortas of our mice with early CKD expressed evidence of osteoblastic transition. The critical osteoblast transcription factor, Runx2 has been shown to be expressed in calcifying vessels and serves as the hallmark of osteoblastic transition of cells in the vasculature. We found Runx2 to be strongly expressed in the aortas of our CKD-2-28 mice (Figure 5A). Furthermore, since osteocytes differentiate from osteoblasts, and osteocytes are the main source of FGF23, we examined aortas for FGF23 expression. As shown in Figure 5B, there was significant expression of FGF23 in the aortas of our sham operated *ldlr*−/− high fat fed mice which was reduced by CKD-2 induction. Immunohistochemical analysis of aortic FGF23 expression (Figure 5C) revealed occasional cells in the aortic media of sham operated mice positive for FGF23. This was lost in the media of CKD-2 mice, replaced by increased advential staining of unknown nature. An advential reaction was also detected when a nonspecific IgG (Total IgG) was used in place of the primary antibody (Figure 5C), but it was clearly distinct from the strong reactivity induced by CKD. Since the advential reaction exactly matched the immunolocalization of FGFR1 (not shown), one possibility is that this reaction represented FGF23 from the circulation bound to its receptor. The expression of the FGF23/klotho hormonal axis in the aorta was further examined by analysis of klotho expression in the aorta. As shown in Figure 5A, there was significant expression of klotho in the sham operated control mice, and induction of CKD-2 markedly decreased klotho expression. These results are in agreement with the recent findings of klotho expression in human vascular media by Lim et al.[32] As shown in Figure 5C, compared to FGF23 which was expressed in occasional cells and decreased by CKD stage 2, α-klotho was strongly expressed in the media of aortas of wild type and sham operated *ldlr*−/− high fat fed mice, and severely depressed in the media of mice with CKD stage 2. In contrast to the reduction in α-klotho in the vasculature, the circulating hormonal form of klotho, cut klotho or c-klotho, which derives from proteolytic cleavage of renal distal tubular α-klotho,[39] was elevated several fold in the CKD-2 mice (Figure 5D).

The skeletons of the CKD-2-28 mice were analyzed by microCT scanning and histomorphometry of trabecular bone. Significant trabecular osteodystrophy was discovered in the *ldlr*−/− high fat fed sham operated mice which produced a decrease in trabecular bone volume and trabecular number and thickness (supplemental Figure 1). The osteodystrophy was affected by CKD-2-28 through a decrease in total area. Histomorphometric analysis confirmed the osteodystrophy of the sham operated *ldlr*−/− high fat fed mice, and

demonstrated the effects of CKD-2-28. Bone formation rates/bone surface were 2.29±1.49 mm^3/cm^2/yr in 28 week old wild-21type C57Bl6J mice used as the normal reference. They were 1.64±0.67 mm^3/cm^2/yr in the sham operated *ldlr*−/− high fat fed control mice, and 0.87 mm^3/cm^2/yr in the CKD-2-28 mice (p<0.05 compared to the sham).

A cortical bone osteodystrophy was also observed by microCT in the *ldlr*−/− high fat fed sham operated mice. The osteodystrophy was worsened by the induction of stage 2 CKD characterized by cortical bone thinning (loss of total volume (TV)) and porosity (decrease in BMD) (Figure 6).

In mice undergoing more severe renal ablation and reduction of GFR to levels equal to human stage 3 CKD (CKD-3, and CKD-3-28), the BUN levels were increased to between 35-55 mg/dl (Table 1), and the animals were hypercalcemic. PTH levels in the CKD-3-28 mice were very high compared to the near normal levels observed in CKD-2-28 mice (Table 1). FGF23 levels were significantly more elevated in the CKD-3-28 mice than in the CKD-2-28 mice using the intact hormone assay, while the C-terminal assay results were similar to CKD-2-28 values (Figure 3C&D). CKD-3-28 significantly increased the number and size of aortic neointimal plaque calcifications without prominent media calcification detected on alizarin red (supplemental Figure 2A) or vonKossa staining (not shown) of aortic sections. Aortic Ca content of CKD-3-28 mice was significantly increased compared to the sham operated control mice, and above the levels found in the aortas of CKD-2-28 mice (supplemental Figure 2B).

Finally, we examined the levels of another supposed osteocytic biomarker protein implicated in CKD and the CKD-MBD to correlate with bone turnover, sclerostin.[40] As shown in supplemental Figure 3, sclerostin levels were significantly increased in the CKD-2-28 mice, more so than in the CKD-3-28 mice.

DISCUSSION

The studies presented here demonstrate that CKD stimulated vascular calcification begins early in the disease. In our model of early kidney disease in the *ldlr*−/− high fat fed atherosclerotic mouse, reduction of GFR equivalent to stage 2 human CKD was associated with a significant increase in aortic Ca content demonstrating vascular calcification. The vascular calcification was early as histological staining did not reveal clear evidence of medial Ca deposition, and the extensive lesions seen in mice with more severe CKD on high Pi diets were not detected.[15] Our results show the onset of CKD stimulated vascular calcification prior to hyperphosphatemia and without high phosphate intake employed by El-Abbadi et al. In addition, they demonstrate the development of vascular calcification earlier than the greater than 40% reduction in GFR suggested by Moe et al.[6] Examination of atherosclerotic plaques failed to demonstrate the extensive Ca deposits stimulated by CKD stage 3/4 we have previously reported,[14, 29, 33] although neointimal plaque Ca deposits were increased in the CKD-3 mice shown here in supplemental Figure 2. Thus, the vascular calcification stimulated in our model by mild CKD is early and most likely amenable to intervention, because visibly detectable deposits would not have to be reversed.

Key mechanisms of vascular calcification were shown to be present in the aortas of normophosphatemic mice with early CKD (CKD-2). Mesenchymal transition to the osteoblastic lineage in the arterial tree is a well-established mechanism of CKD stimulated vascular calcification,[13, 36, 37, 41] and vascular Runx2 expression has become its hallmark biomarker.[42] Runx2 expression in the aortic media of was increased in our CKD-2 mice compared to the *ldlr*–/–high fat fed sham operated controls. A new key pathogenetic mechanism of vascular calcification in CKD, reduction of medial αklotho activity,[30, 32] was demonstrated in the aortic media of the CKD-2 mice by Westerns, histology and message levels. Since klotho antagonizes endothelial injury,[43] these findings may suggest an underappreciated role of endothelial injury in our model and in CKD stimulated vascular calcification. Our results agree with early reduction of renal klotho shown by Hu et al,[30] but their studies suggested that the function of vascular klotho was inhibition of the phosphate stimulation of vascular calcification, while our studies show that CKD stimulation of vascular calcification is prior to disruption of phosphate homeostasis. The FGFR/α-klotho ligand, FGF23, was found surprisingly induced in the aortic media of the sham operated *ldlr* –/– high fat fed mice and decreased by CKD-2. CKD-2 also stimulated an FGF23 advential immunolocalization reaction that may have represented circulating FGF23 bound to receptors. The localization of FGF23 suggests that osteocytic differentiation which stems from osteoblasts may have been the mechanism of FGF23 expression in agreement with the findings of Zhu et al,[44] and that the increase in FGF23 expression may represent a defense against vascular calcification as first suggested by Voigt et al.[31] Scialla et al found in the CRIC cohort that FGF23 levels were not associated with vascular calcification (Scialla et al, KI in press). Our studies are one of the first to report CKD stimulated vascular FGF23 expression, specifically in the aorta. This establishes a potential paracrine role of FGF23 interacting with medial klotho/FGFR. The reduction of klotho expression in the aortic media in CKD stage 2 mice indicates a potential resistance to FGF23 actions in the vasculature and raises the issue of the role of FGF23 in vascular calcification which was not able to be addressed in the present studies. Lim et al,[32] recently reported that reduction of vascular klotho contributes to vascular calcification and causes resistance to the actions of FGF23 which, though not characterized, were thought to be resistive to vascular calcification. Lim et al and Donate-Correa et al[43] did not find evidence for vascular FGF23 expression though others have[31] in agreement with our results.

The picture of the CKD-MBD syndrome in early CKD shows multiple evidences of skeletal effects produced by kidney disease. Our results demonstrated inhibition of bone formation rates, a decrease in cortical bone mineral density, a decreased bone area and increased osteocytic secretion in the CKD-2 mice. Sabbagh et al,[21] demonstrate that reduction of nuclear β-catenin, a manifestation of decreased Wnt signaling and decreased skeletal anabolism was the earliest detected skeletal abnormality in CKD, and Pereira et al,[19] showed that FGF23 levels derived from skeletal osteocytes was increased in stage 2 CKD. Clinical and translational studies in models other than that used here and by Fang et al,[20] fail to demonstrate the decrease in bone formation reported in our studies. Rather, they show gradual development of high turnover osteodystrophy compatible with the effects of increased parathyroid hormone (PTH).[6, 21, 45, 46] The likely explanation for this is the restriction to osteoblastogenesis imposed by the high PPARγ activity in our model.[47] The

resultant resistance to adaptive stimulation of bone formation by parathyroid hormone permits the effects of kidney injury to inhibit bone formation to be observed in our model despite the development of secondary hyperparathyroidism. Despite the absence of a decrease in bone formation in early CKD, studies by Sabbagh et al,[21] indicate that decreased skeletal Wnt signaling is the earliest manifestation of the CKD-MBD detected in the *jck* mouse, a model of polycystic kidney disease, despite their observation of a gradual onset of high turnover renal osteodystrophy by stage 3 CKD. Thus, early CKD affects the skeleton, and this may represent the onset of the CKD-MBD. The effects of early CKD on the skeleton showed here produced a low turnover osteodystrophy and a decrease in cortical bone mineral density. Because of the still poorly characterized "bone-vascular axis", our findings of this osteodystrophy have to be considered in the pathogenetic mechanisms of the vascular calcification we demonstrate to be stimulated by early CKD.

Two markers of osteocytic secretory activity, FGF23 and sclerostin, were increased in the CKD-2 mice. Activation of osteocytic FGF23 secretion is thought to be phosphate dependent, but the location of the sensing mechanism was unknown and FGF23 regulation in normophosphatemia unexplained. The recent discovery of the hormonal role of the cleavage product produced by proteolytic cleavage of the extracellular domain of α-klotho clarifies that the distal tubule sensing increased phosphate delivery and producing c-klotho may be a mechanism of stimulating FGF23 secretion in early CKD in the presence of normal serum phosphate.[39] We found that c-klotho levels were elevated in the CKD-2 mice compatible with the marked increase in FGF23 and the normal serum phosphate. Several studies such as those of Seiler et al[48] suggest that c-klotho levels decline during CKD in concert with loss of renal αklotho expression. However, our model of CKD-2 results from hypertrophy of a remnant kidney following acute kidney injury. The loss of αklotho occurring during the kidney injury phase is recovered during hypertrophy as shown in the immunohistochemistry of the CKD-2 kidneys (supplemental Figure 4). Thus, there is sufficient αklotho substrate for the production of c-klotho by tubular phosphate stimulated ADAM-17 and -10. Thus, our results are one of the first to suggest that in early CKD prior to hyperphosphatemia, the mechanism of increased FGF23 secretion may be mediated by cklotho. The complex situation of the kinetics of klotho expression in the face of decreased transcription and increased proteolytic cutting by ADAMS-17 and -10 require careful study. In addition, the effects of tubular phosphate on ADAMS-17 and -10 activity require further study.

The novel findings reported here are staging of CKD by BUN and inulin clearances in mice; the stimulation of vascular calcification by CKD equivalent to human stage II CKD (CKD-2 mice) prior to hyperphosphatemia; reduction of vascular αklotho in early CKD; increased c-klotho as a means to increased FGF23 secretion in normophosphatemic CKD; and increased sclerostin levels and inhibition of bone formation in early CKD. In conclusion, early CKD induced in a model of atherosclerosis, stimulated vascular calcification, stimulated mesenchymal osteoblastic transition in the vasculature, inhibited bone formation, elevated FGF23 and sclerostin levels, and decreased aortic medial klotho expression. Ca and Pi levels were normal in early CKD, and PTH levels increased by acute kidney injury tended to normalize in CKD stage 2 while FGF23 levels continued to increase.

Methods

Induction of CKD

A two-step procedure was utilized to create chronic kidney disease as described previously.[1, 2] Electrocautery was applied to the right kidney through a 2 cm flank incision at 12 weeks post natal, followed by left total nephrectomy through a similar incision 2 weeks later. The intensity of the cautery was varied to produce mild (CKD-2) or moderate (CKD-3) renal injury that was confirmed by inulin clearances at age 26 weeks. Control animals received sham operations in which the appropriate kidney was exposed and mobilized but not treated in any other way. After the surgical procedures, 14-week-old mice were randomized into groups. The first was wild type mice fed a regular diet. This was the normal renal function and diet group. The second group was *ldlr−/−* mice that were fed a high fat diet and sham operated. This group had normal renal function. This group served as the control group to determine the effect of high fat diet in the face of normal renal function. The third group was *ldlr−/−* mice with GFR reduced equivalent to human CKD stage 2 fed high fat diet (CKD-2) and sacrificed at 22 weeks, the baseline group (22 weeks). The fourth group was *ldlr−/−* mice with CKD-2 sacrificed at 28 weeks, (28 weeks). The fifth group was *ldlr−/−* mice with GFR reduced equivalent to human CKD stage3 fed high fat diet (CKD-3) and sacrificed at 22 weeks, the baseline group for the CKD-3. The sixth group was *ldlr−/−* mice with CKD-3 sacrificed at 28 weeks. Once the mice were randomized into groups, they were allowed to develop calcification from weeks 14 through 22 weeks post natal. Interventions can be initiated at 22 weeks in treatment protocols, and continued until week 28 postnatal at which time the mice are sacrificed under anesthesia. Intraperitoneal anesthesia (xylazine 13 mg/kg and ketamine 87 mg/kg) was used for all procedures. Saphenous vein blood samples were taken 1 week following the second surgery to assess baseline post-surgical renal function. At the time of sacrifice, blood was taken by intracardiac stab, and the heart and aorta dissected en bloc.

Chemical Calcification Quantitation

Aorta and Hearts were dissected at sacrifice, and all extraneous tissue removed by blunt dissection under a dissecting microscope. Tissues were desiccated for 20-24 hours at 60° C, weighed and crushed to a powder with a pestle and mortar. Calcium was eluted in 1N HCL for 24 hours at 4°C. Calcium content of eluate was assayed using a cresolphthalein complexone method (Sigma, St Louis), according to manufacturer's instructions, and results were corrected for dry tissue weight.

Blood tests

Serum was analyzed on the day of blood draw for blood urea nitrogen (BUN), calcium, and phosphate by standard autoanalyzer laboratory methods performed by our animal facility. Parathyroid hormone levels in plasma were measured using a PTH (mouse, Intact) ELISA kit (ALPCO Diagnostics, Salem, NH 03079). This is a two-site enzyme -linked immunosorbent assay performed according to manufacturer's recommendations. The absorbance was read at 450 nm using a microplate reader (Molecular Devices, VERSA max). FGF23 levels were measured by two separate assays, the Kainos intact hormone assay (Kainos, Tokyo Japan), and a C-terminal assay (Immunotopics, Stillwater, MN). The

circulating c-klotho levels were measured by an ELISA (MyBioSource.COM, San Diego, CA, #MBS702609). The Sclerostin levels were analyzed using a sandwich enzyme immunoassay kit (# ABIN426039, Antibodies – online Inc, Atlanta, GA, USA) for the in vitro quantitative measurement of SOST in mouse plasma. For the Elisa assays blood was drawn by saphenous vein or cardiac puncture at the time of euthanasia. All blood samples were placed on ice at collection. Platelet poor EDTA plasma samples were made by a 2-step centrifugation at 6000 rpm for 5 minutes and 14000 rpm for 2 minutes both at 4°C. Samples were stored frozen at – 20°C or below until being used.

Histology and immunohistochemistry

Aortic tissues were fixed in 10% neutral buffered formalin overnight, then transferred to 70% ethanol at 4 °C and embedded in paraffin. Five micron sections were prepared. Alizarin red staining was used to detect calcification, according to a standard protocol [3]. For Immunohistochemical staining, all slides were deparaffinized in xylene and dehydrated in a graded ethanol series and then rehydrated. Endogenous peroxidase was blocked with 3% H_2O_2 in methanol for 15 min. Non-specific binding was blocked with avidin and biotin blocking agents (Vector laboratories, Burlingame, CA, USA) for 30 min, then with 5% normal donkey serum for 10 min. After washing with PBS, the slides were incubated with primary antibody at 4 °C overnight, and followed by incubation with biotinylated secondary antibody (Vector laboratories) at room temperature for one hour, then the strepatividin – conjugated perioxidase staining was performed using DAB kit (SK-4100, Vector laboratories) and ImmPACT ™ AEC kit (SK -4205, Vector laboratories), respectively. The species – specific total Ig (Vector laboratories), and monoclonal anti -mouse FGF-23 antibody (Catalog # MAB26291), polyclonal anti -mouse klotho antibody (catalog#AF1819) and Monoclonal anti -human/mouse RUNX2/CBFA1 antibody (catalog # MAB2006), (R&D systems, Inc. Minneapolis, MN, USA), were utilized in this study.

RT-PCR

RNA was extracted from aortas and cell cultures using RNeasy Mini Kits (Qiagen, Valencia, CA). 1 μg of total RNA was reverse transcribed using iScript cDNA synthesis kit from Bio-Rad (Hercules, Ca) according to manufacturer's instructions. Primers were designed using Vector NTI software (Invitrogen, Grand Island, NY) and optimal conditions for each prime pairs were determined. A Perkin-Elmer DNA Thermal Cycler was used to perform the reaction. Following reverse transcription performed as above, real time was performed using the MX 4000 (Strategene, La Jolla, CA), SYBR Green from Sigma (St. Louis) and the PCR kit from Invitrogen. Each reaction was performed in triplicate at 95°C, 45 sec, and 60°C, 30 sec, and 60 sec at 72°C for 40 cycles. This was followed by a melt cycle, which consisted of stepwise increase in temperature from 72°C to 99°C. A single predominant peak was observed in the dissociation curve of each gene, supporting the specificity of the PCR product. Ct numbers (threshold values) were set within the exponential phase of PCR and were used to calculate the expression levels of the genes of interest. GAPDH was used as an internal standard and used to normalize the values. A standard curve consisting of the c_T versus log cDNA dilutions (corresponding to the log copy numbers) was generated by amplifying serial dilutions of cDNA corresponding to an unknown amount of amplicon.

Negative controls were performed by inactivating the reverse transcriptase by boiling for 5 min prior to RT-PCR to insure that genomic DNA was not amplified.

Bone Histology and Histomorphometry

Bone formation rate/bone surface was determined at the time of sacrifice. All mice received intraperitoneal tetracycline (5 mg/kg) 7 and 2 days before being sacrificed. Both femurs were dissected at the time of sacrifice and placed in 70% ethanol. All bone samples were dehydrated, and embedded in methylmethacrylate as previously described.[4] Serial sections of 4- and 7-μm thicknesses were cut with a Microm microtome (model HM360, C. Zeiss, Thornwood, NY). Sections were stained with the modified Masson-Goldner trichrome stain.[5] Unstained sections were prepared for phase contrast and fluorescent light microscopy.

Histomorphometric parameters of bone were evaluated at standardized sites in cancellous bone using the semiautomatic method (Osteoplan II, Kontron, Munich, Germany) at a magnification of 200×.[6, 7] The histomorphometric parameters comply with the guidelines of the nomenclature committee of the American Society of Bone and Mineral Research.[8] Osteoplan II software has been programmed to transfer data automatically to statistical software (SPSS for Windows; Chicago Ill).

Statistical Analyses

Statistical analysis was performed using ANOVA. Differences between groups were assessed post hoc using Fisher LSD method and considered significant at $p < .05$. Data are presented as mean $\pm$ SE. Analyses were performed using Sigma Stat statistical software (Point Richmond, CA).

Supplementary Material

Refer to Web version on PubMed Central for supplementary material.

Acknowledgments

REFERENCES

1. Moe S, Drueke T, Cunningham J, et al. Definition, evaluation, and classification of renal osteodystrophy: A position statement from Kidney Disease: Improving Global Outcomes (KDIGO). Kidney Int. 2006; 69:1945–1953. [PubMed: 16641930]

2. Go AS, Chertow GM, Fan D, et al. Chronic kidney disease and the risks of death, cardiovascular events, and hospitalization. New Engl J Med. 2004; 351:1296–1305. [PubMed: 15385656]

3. Block GA, Hulbert-Shearon TE, Levin NW, et al. Association of serum phosphorus and calcium × phosphate product with mortality risk in chronic hemodialysis patients: a national study. Am J Kidney Dis. 1998; 31:607–617. [PubMed: 9531176]

4. Kestenbaum B, Sampson JN, Rudser KD, et al. Serum phosphate levels and mortality risk among people with chronic kidney disease. J Am Soc Nephrol. 2005; 16:520–528. [PubMed: 15615819]

5. Keith DS, Nichols GA, Gullion CM, et al. Longitudinal follow-up and outcomes among a population with chronic kidney disease in a large managed care organization. Arch Intern Med. 2004; 164:659–663. [PubMed: 15037495]

6. Moe SM, Radcliffe JS, White KE, et al. The pathophysiology of early-stage chronic kidney disease–mineral bone disorder (CKD-MBD) and response to phosphate binders in the rat. J Bone Miner Res. 2011; 26:2672–2681. [PubMed: 21826734]

7. Blacher J, Guerin AP, Pannier B, et al. Arterial calcifications, arterial stiffness, and cardiovascular risk in end-stage renal disease. Hypertension. 2001; 38:938–942. [PubMed: 11641313]

8. London GM, Guerin AP, Marchais SJ, et al. Arterial media calcification in end-stage renal diseases: impact on all-cause and cardiovascular mortality. Nephrol Dial Transplant. 2003; 18:1731–1740. [PubMed: 12937218]

9. Hruska K, Mathew S, Lund R, et al. Cardiovascular risk factors in chronic kidney disease: does phosphate qualify? Kidney Int. 2011; 79(Suppl 121):S9–S13. [PubMed: 26746860]

10. Gutierrez OM, Mannstadt M, Isakova T, et al. Fibroblast Growth Factor 23 and Mortality among Patients Undergoing Hemodialysis. New Engl J Med. 2008; 359:584–592. [PubMed: 18687639]

11. Arnlov J, Carlsson AC, Sundstrom J, et al. Higher fibroblast growth factor-23 increases the risk of all-cause and cardiovascular mortality in the community. Kidney Int. 2013; 83:160–166. [PubMed: 22951890]

12. Rennenberg RJMW, Kessels AGH, Schurgers LJ, et al. Vascular calcifications as a marker of increased cardiovascular risk: a meta-analysis. Vasc Health Risk Manag. 2009; 5:185–197. [PubMed: 19436645]

13. Moe SM, Chen NX. Pathophysiology of Vascular Calcification in Chronic Kidney Disease. Circulation Research. 2004; 95:560–567. [PubMed: 15375022]

14. Mathew S, Lund R, Strebeck F, et al. Reversal of the adynamic bone disorder and decreased vascular calcification in chronic kidney disease by sevelamer carbonate therapy. J Am Soc Nephrol. 2007; 18:122–130. [PubMed: 17182886]

15. El-Abbadi MM, Pai AS, Leaf EM, et al. Phosphate feeding induces arterial medial calcification in uremic mice: role of serum phosphorus, fibroblast growth factor-23, and osteopontin. Kidney Int. 2009; 75:1297–1307. [PubMed: 19322138]

16. Chen NX, O'Neill KD, Duan D, et al. Phosphorus and uremic serum up-regulate osteopontin expression in vascular smooth muscle cells. Kidney Int. 2002; 62:1724–1731. [PubMed: 12371973]

17. Shanahan CM, Crouthamel MH, Kapustin A, et al. Arterial calcification in chronic kidney disease: Key roles for calcium and phosphate. Circ Res. 2011; 109:697–711. [PubMed: 21885837]

18. Hill KM, Martin BR, Wastney ME, et al. Oral calcium carbonate affects calcium but not phosphorus balance in stage 3-4 chronic kidney disease. Kidney Int. 2012

19. Pereira RC, Juppner H, Azucena-Serrano CE, et al. Patterns of FGF-23, DMP1 and MEPE expression in patients with chronic kidney disease. Bone. 2009; 45:1161–1168. [PubMed: 19679205]

20. Fang Y, Zhang Y, Mathew S, et al. Early chronic kidney disease (CKD) stimulates vascular calcification (VC) and decreased bone formation rates prior to positive phosphate balance. J Am Soc Nephrol. 2009; 20:36A.

21. Sabbagh Y, Graciolli FG, O'Brien S, et al. Repression of osteocyte Wnt/β-catenin signaling is an early event in the progression of renal osteodystrophy. J Bone Miner Res. 2012; 27:1757–1772. [PubMed: 22492547]

22. Oliveira RB, Cancela ALE, Graciolli FG, et al. Early Control of PTH and FGF23 in Normophosphatemic CKD Patients: A New Target in CKD-MBD Therapy? Clin J Am Soc Nephrol. 2010; 5:286–291. [PubMed: 19965540]

23. Isakova T, Wahl P, Vargas GS, et al. Fibroblast growth factor 23 is elevated before parathyroid hormone and phosphate in chronic kidney disease. Kidney Int. 2011; 79:1370–1378. [PubMed: 21389978]

24. Babij P, Zhao W, Small C, et al. High bone mass in mice expressing a mutant LRP5 gene. J Bone Miner Res. 2003; 18:960–974. [PubMed: 12817748]

25. Little RD, Carulli JP, DelMastro RG, et al. A mutation in the LDL receptor-related protein 5 gene results in the autosomal dominant high-bone-mass trait. Am J Hum Genet. 2002; 70:11–19. [PubMed: 11741193]

26. Lund RJ, Davies MR, Brown AJ, et al. Successful treatment of an adynamic bone disorder with bone morphogenetic protein-7 in a renal ablation model. J Am Soc Nephrol. 2004; 15:359–369. [PubMed: 14747382]

27. Mahmoodi BK, Matsushita K, Woodward M, et al. Associations of kidney disease measures with mortality and end-stage renal disease in individuals with and without hypertension: a meta-analysis. The Lancet.

28. Fox CS, Matsushita K, Woodward M, et al. Associations of kidney disease measures with mortality and end-stage renal disease in individuals with and without diabetes: a meta-analysis. The Lancet.

29. Davies MR, Lund RJ, Hruska KA. BMP-7 is an efficacious treatment of vascular calcification in a murine model of atherosclerosis and chronic renal failure. J Am Soc Nephrol. 2003; 14:1559–1567. [PubMed: 12761256]

30. Hu MC, Shi M, Zhang J, et al. Klotho Deficiency Causes Vascular Calcification in Chronic Kidney Disease. J Am Soc Nephrol. 2011; 22:124–136. [PubMed: 21115613]

31. Voigt M, Fischer D-C, Rimpau M, et al. Fibroblast growth factor (FGF)-23 and fetuin-A in calcified carotid atheroma. Histopathology. 2010; 56:775–788. [PubMed: 20546343]

32. Lim K, Lu TS, Molostvov G, et al. Vascular Klotho Deficiency Potentiates the Development of Human Artery Calcification and Mediates Resistance to Fibroblast Growth Factor 23 / Clinical Perspective. Circulation. 2012; 125:2243–2255. [PubMed: 22492635]

33. Davies MR, Lund RJ, Mathew S, et al. Low turnover osteodystrophy and vascular calcification are amenable to skeletal anabolism in an animal model of chronic kidney disease and the metabolic syndrome. J Am Soc Nephrol. 2005; 16:917–928. [PubMed: 15743994]

34. Ben-Dov IZ, Galitzer H, Lavi-Moshayoff V, et al. The parathyroid is a target organ for FGF23 in rats. J Clin Invest. 2007; 117:4003–4008. [PubMed: 17992255]

35. London GM. Cardiovascular Calcifications in Uremic Patients: Clinical Impact on Cardiovascular Function. Journal of the American Society of Nephrology. 2003; 14:S305–S309. [PubMed: 12939386]

36. Mathew S, Tustison KS, Sugatani T, et al. The mechanism of phosphorus as a cardiovascular risk factor in chronic kidney disease. J Am Soc Nephrol. 2008; 19:1092–1105. PMCID:PMC2396927. [PubMed: 18417722]

37. Speer MY, Yang HY, Brabb T, et al. Smooth muscle cells give rise to osteochondrogenic precursors and chondrocytes in calcifying arteries. Circ Res. 2009; 104:733–741. [PubMed: 19197075]

38. Shanahan CM, Cary NRB, Salisbury JR, et al. Medial localization of mineralization-regulating proteins in association with Monckeberg's sclerosis: Evidence for smooth muscle cell-mediated vascular calcification. Circulation. 1999; 100:2168–2176. [PubMed: 10571976]

39. Smith RC, O'Bryan LM, Farrow EG, et al. Circulating α-Klotho influences phosphate handling by controlling FGF23 production. J Clin Invest. 2012; 122:4710–4715. [PubMed: 23187128]

40. Cejka D, Herberth J, Branscum AJ, et al. Sclerostin and Dickkopf-1 in Renal Osteodystrophy. Clin J Am Soc Nephrol. 2011; 6:877–882. [PubMed: 21164019]

41. Shanahan CM, Proudfoot D, Tyson KL, et al. Expression of mineralisation-regulating proteins in association with human vascular calcification. Zeitschrift fur Kardiologie. 2000; 89:S063–S068.

42. Moe SM, O'Neill KD, Duan D, et al. Medial artery calcification in ESRD patients is associated with deposition of bone matrix proteins. Kidney International. 2002; 61:638–647. [PubMed: 11849407]

43. Donate-Correa J, Mora-Fernández C, Martínez-Sanz R, et al. Expression of FGF23/KLOTHO system in human vascular tissue. Int J Cardiology. 2011

44. Zhu D, Mackenzie NCW, Millán JL, et al. The Appearance and Modulation of Osteocyte Marker Expression during Calcification of Vascular Smooth Muscle Cells. PLoS ONE. 2011; 6:e19595. [PubMed: 21611184]

45. Slatopolsky E, Caglar S, Pennell JP. On the pathogensis of hyperparathyroidism in chronic experimental insufficiency in the dog. J Clin Invest. 1971; 50:492–499. [PubMed: 5545116]

46. Stubbs JR, He N, Idiculla A, et al. Longitudinal evaluation of FGF23 changes and mineral metabolism abnormalities in a mouse model of chronic kidney disease. J Bone Miner Res. 2012; 27:38–46. [PubMed: 22031097]

47. Lecka-Czernik B, Gubrij I, Moerman EJ, et al. Inhibition of Osf2/Cbfa1 expression and terminal osteoblast differentiation by PPAR g 2. J Cellular Biochem. 1999; 74:347–371.

48. Seiler S, Wen M, Roth HJ, et al. Plasma Klotho is not related to kidney function and does not predict adverse outcome in patients with chronic kidney disease. Kidney Int. 2013; 83:121–128. [PubMed: 22895520]

References

1. Davies MR, Lund RJ, Hruska KA. BMP-7 is an efficacious treatment of vascular calcification in a murine model of atherosclerosis and chronic renal failure. J Am Soc Nephrol. 2003; 14:1559–1567. [PubMed: 12761256]

2. Davies MR, Lund RJ, Mathew S, et al. Low turnover osteodystrophy and vascular calcification are amenable to skeletal anabolism in an animal model of chronic kidney disease and the metabolic syndrome. J Am Soc Nephrol. 2005; 16:917–928. [PubMed: 15743994]

3. Gregory CA, Grady Gunn W, Peister A, et al. An Alizarin red-based assay of mineralization by adherent cells in culture: comparison with cetylpyridinium chloride extraction. Analytical Biochemistry. 2004; 329:77–84. [PubMed: 15136169]

4. Malluche, HH.; Faugere, MC. Atlas of Mineralized Bone Histology. Karger; New York: 1986.

5. Goldner J. A modification of the Masson trichrome technique for routine laboratory purposes. Am J Pathol. 1938; 14:237–243. [PubMed: 19970387]

6. Malluche HH, Sherman DR, Meyer W, et al. A new semiautomatic method for quantitative static and dynamic bone histology. Calcif Tissue Int. 1982; 34:439–448. [PubMed: 6817891]

7. Manaka RC, Malluche HH. A program package for quantitative analysis of histologic structure and remodeling dynamics of bone. Comput Programs Biomed. 1981; 13:191–202. [PubMed: 7032836]

8. Parfitt AM, Drezner MK, Glorieux FH, et al. Bone histomorphometry: Standardization of nomenclature, symbols, and units. J Bone Miner Res. 1987; 2:595–610. [PubMed: 3455637]
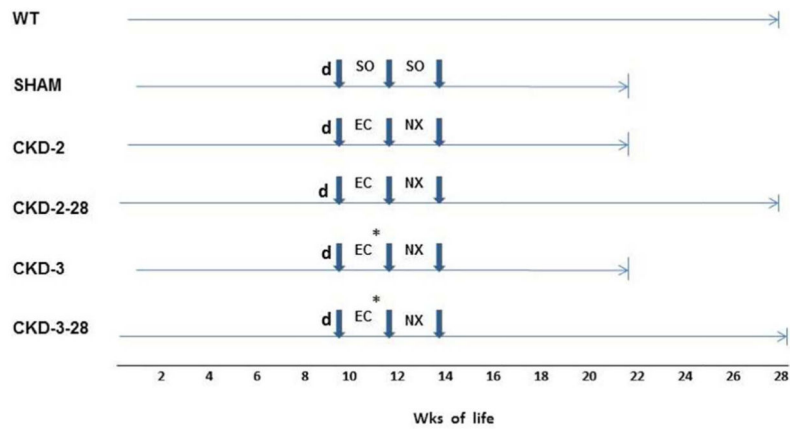
Figure 1. A Schematic Drawing of the Experimental Design Defining the Various Animal Groups
WT, wild type C57B6J mice were used to establish normative parameters; SHAM, *ldlr−/−* mice on a high fat diet (d) undergoing sham operations (SO) are the control mice for the effects of CKD; CKD-2, *ldlr−/−* high fat fed mice undergoing mild renal injury (EC) and contralateral nephrectomy (NX) with euthanasia at 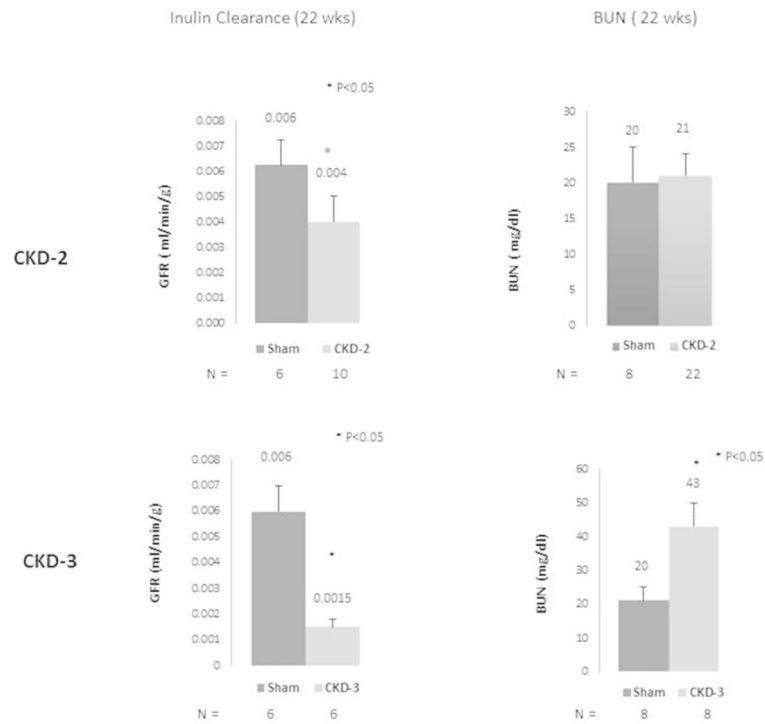22 weeks; CKD-2-28, same as CKD-2 but euthanasia at 28 weeks, (six additional weeks of slowly progressive CKD); CKD-3, *ldlr −/−* high fat fed mice undergoing moderate renal injury (EC*) and contralateral nephrectomy (NX) with euthanasia at 22 weeks; CKD-3-28, same as CKD-3 but euthanasia at 28 weeks.

Figure 2. Inulin clearances in *ldlr−/−* high fat fed mice

Sham operated mice had inulin clearances of 0.006mls/min/g. The mild renal injury group (CKD-2) had reductions in inulin clearance (GFR) up to 40% (mean 33%) of the sham operated control levels,. The BUN levels were not different between sham operated and CKD-2 mice, More severe renal injury (CKD-3) produced inulin clearance reductions of 75% in CKD-3 mice and elevations in BUN levels to the 45mg/dl range. Inulin clearances and BUN levels were determined at 22 weeks of age.
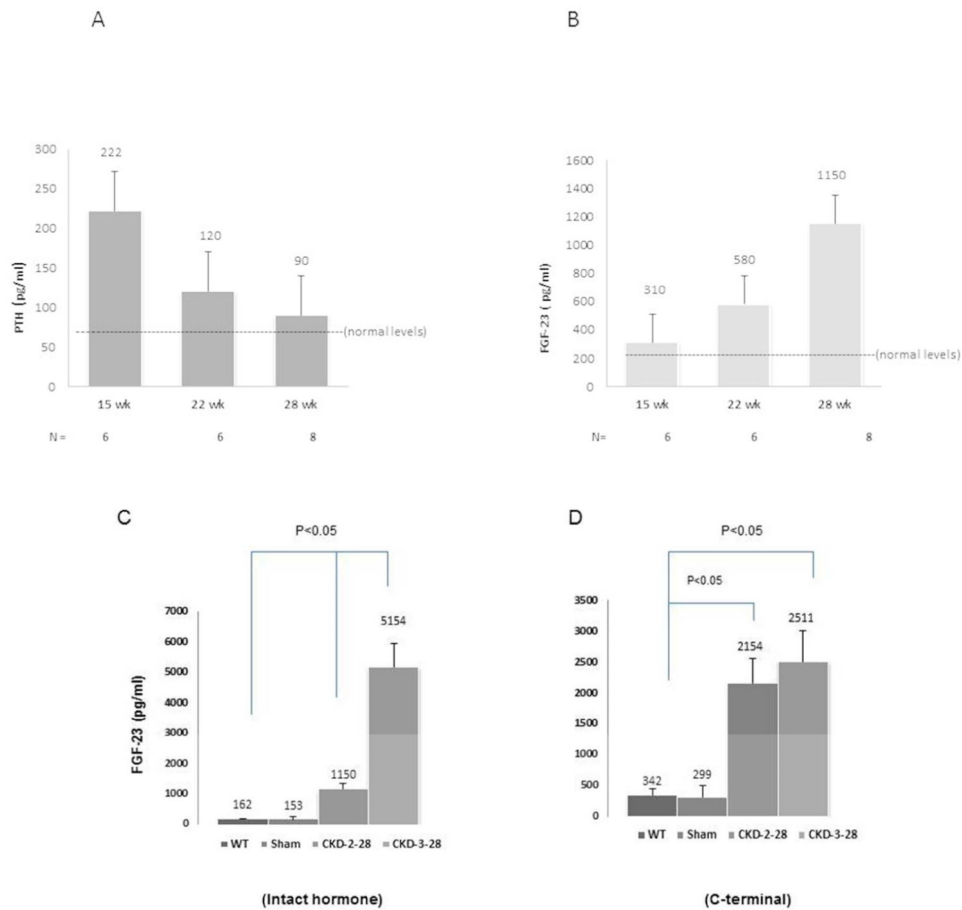
Figure 3. Longitudinal analysis of parathyroid hormone (PTH) and fibroblast growth factor 23 (FGF23) levels in *ldlr*−/− high fat fed mice with CKD-2 and CKD-2-28, and FGF23 levels in *ldlr* −/− high fat fed mice with CKD-2-28 and CKD-3-28. A and B

CKD was established at 14 weeks of age as described in methods and Fig.1. Plasma was obtained at 15, 22, and 28 weeks. FGF23 was measured using an intact hormone assay (Kainos). C and D, Two different Elisa assays for FGF23, an intact hormone assay and a C-terminal assay, as described in methods, were used to determine the effects of CKD on FGF23 levels in the circulation. FGF23 levels in C57Bl6J wild type mice were measured to establish the reference range. FGF23 levels measured using the intact hormone assay were increased in CKD-3-28 mice compared to CKD-2-28, but not when the C-terminal assay was used.
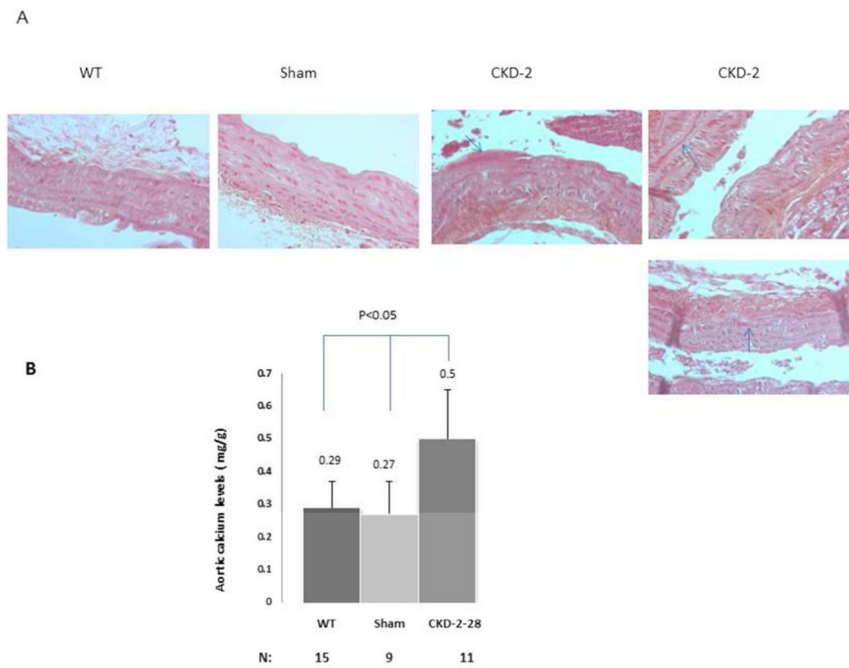
Figure 4. Aortic calcium levels are increased by CKD stage 2-28 in *ldlr−/−* high fat fed mice
A, alizarin red staining revealed questionable early aortic calcium deposition along elastic laminae (arrows) in *ldlr−/−* high fat fed mice with CKD-2-28 compared to sham operated mice. Von Kossa staining of adjacent sections (not shown) was negative. B, CKD-2-28 significantly increased aortic Ca content.
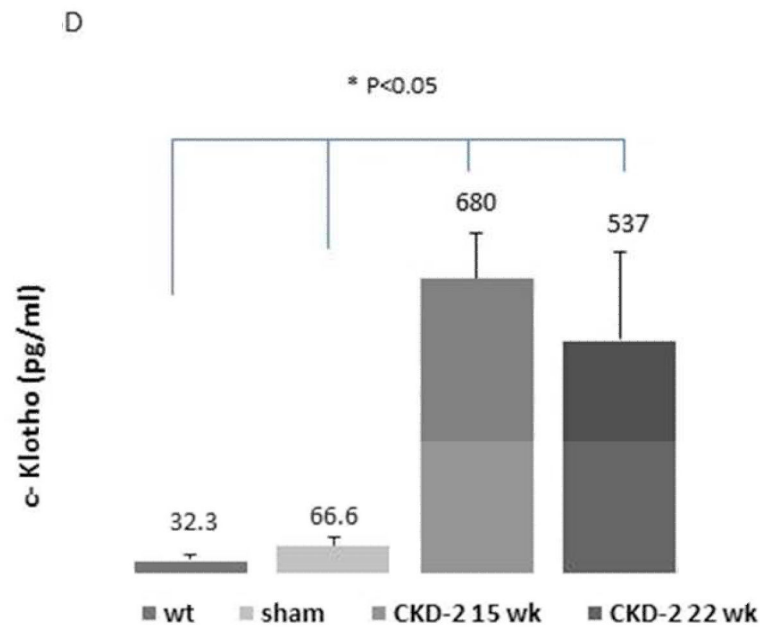
A

B

C

IHC data of CKD mice aorta
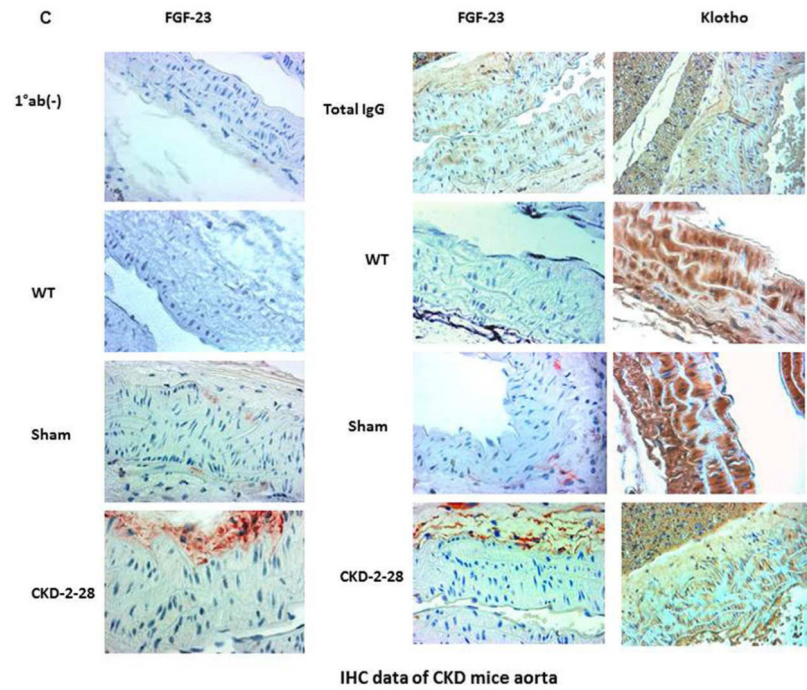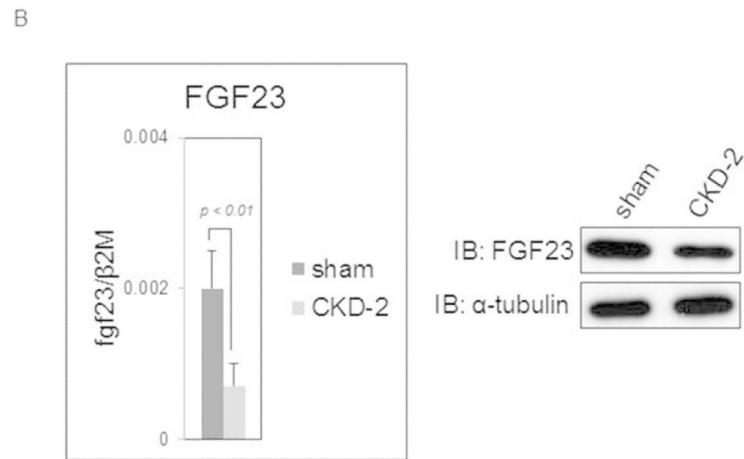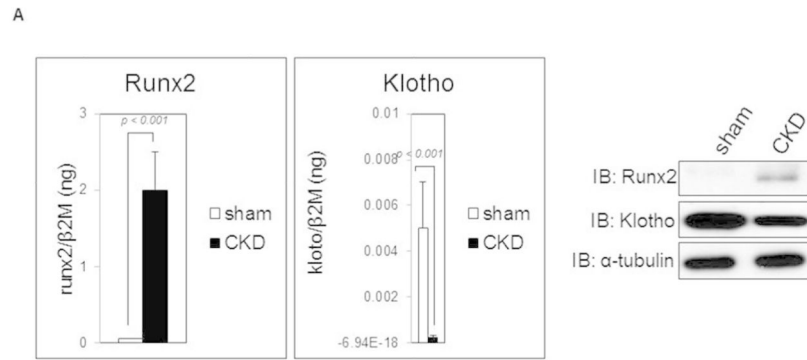
Figure 5. Osteoblastic transition and detection of FGF-23 and klotho expression in aortas of CKD -2-28 *ldlr−/−* mice

Real time PCR (**A &B**) and western blotting were used to measure Runx2, klotho (**A**) and FGF 23 (**B**) expression in aortas of sham and CKD-2-28 mice. Immunolocalization of aortic FGF23 and klotho (**C**). Plasma levels of circulating klotho (c klotho) (**D**). **A,** CKD-2-28 increased Runx2 expression and decreased α-Klotho expression compared to sham operated controls determined by real time RT-PCR (left) and by Western (right). n = 5 for RT-PCR. The representative Westerns were uniform for five CKD-2-28 mice. FGF23 was expressed in the sham operated control mice and decreased with induction of CKD-2-28. n = 5 for RT-PCR. The representative Westerns were uniform for five CKD-2-28 mice. **C,** Antibodies to FGF23 and Klotho, as described in Methods, were used for detection of expression in the aortas of the various groups of mice. FGF23 was expressed in occasional cells in the media (two representative sham mice are shown) which was absent in CKD-2-28 mice. A strong nonspecific advential reaction was increased in the CKD-2-28 mice of unknown nature. α-Klotho was strongly expressed in the aortic media of wild type and sham operated mice, but severely reduced in the stage 2 CKD mice. IHC for α-Klotho was uniform in five WT, Sham, and CKD-2 mice. Use of a nonspecific IgG in place of the primary antibody produced nonspecific positivity by both the secondary antibodies for both FGF23 and klotho. **D,** Plasma c klotho levels were increased several fold in the CKD-2 mice at 15 and 22wks.
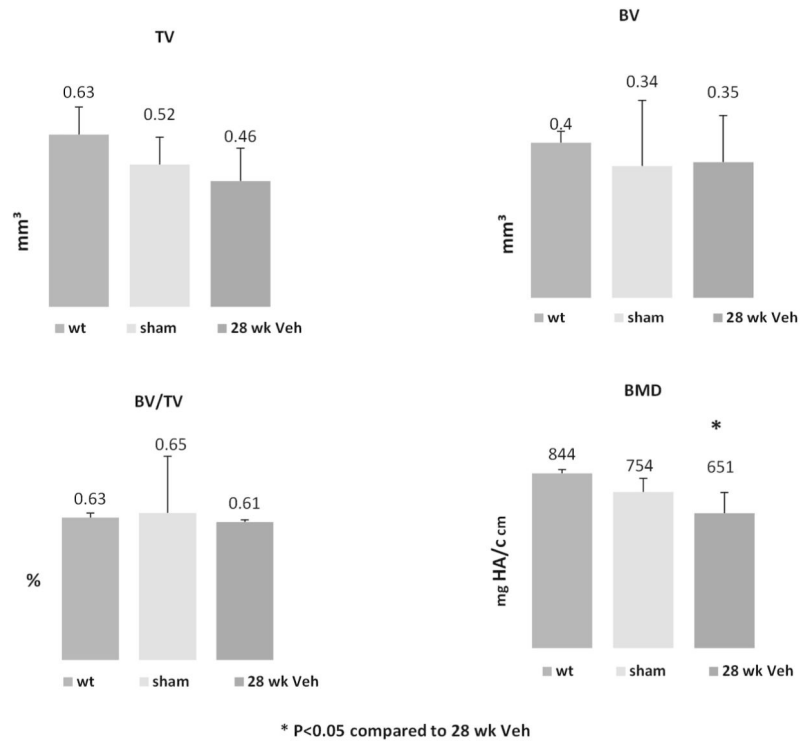
Figure 6. Cortical bone microCT in *ldlr*−/− high fat fed mice with CKD stage 2
There was a decline in TV and in bone mineral density (BMD) in the CKD-2 mice. n = 10

Table 1
Serum and Plasma Chemistries and PTH levels

Experiment Groups	BUN (mg/dl)	Ca (mg/dl)	Pi (mg/dl)	PTH (pg/ml)
WT, wild type C57BL6	22.4 ± 4.6	8.28 ± 1.8	8.85 ± 0.2	70.2 ± 10.9
Sham, *Idlr*−/− high fat	20.6 ± 3.7	8.96 ± 0.8	7.92 ± 2.3	74.5 ± 35.4
CKD-2, *Idlr*−/− high fat (22 wks)	21.1 ± 2.8	7.94 ± 1.2	8.8 ± 3.5	120 ± 48
CKD-2-28 *Idlr*−/− high fat (28 wks)	27.5 ± 4$^{*\#}$	8.8 ± 1.4	12.7 ± 3.9$^{*\#}$	90.8 ± 20
CKD-3 *Idlr*−/− high fat (22 wks)	43.7 ± 7.5$^{*\#}$	10.8 ± 0.7$^{*\#}$	11.78 ± 1.9$^{*\#}$	NA
CKD-3-28 *Idlr*−/− high fat (28 wks)	53.3 ± 13.4$^{*\#}$	11.13 ± 1.5$^{*\#}$	13 ± 2.7$^{*\#}$	467 ± 125$^{*\#}$

Number of animals per group #x201C;N = 8-21"

* p<0.01 compared to sham

$^\#$ p<0.01 compared to CKD-2

$^+$ p<0.01 compared to CKD-2